Manuscript published in Energy **102**, 161–165 (2016)

# Investigation of water transport dynamics in polymer electrolyte membrane fuel cells based on high porous micro porous layers

**Saad S. Alrwashdeh [a,b,c,*], Henning Markötter [a,c], Jan Haußmann [d], Tobias Arlt [a], Merle Klages [d], Joachim Scholta [d], John Banhart [a,c], Ingo Manke [a]**

[a] *Helmholtz-Zentrum Berlin, Hahn-Meitner-Platz 1, 14109 Berlin, Germany*

[b] *Mechanical Engineering Department, Faculty of Engineering, Mu'tah University, P.O Box 7, Al-Karak 61710 Jordan*

[c] *Technische Universität Berlin, Straße des 17. Juni 135, 10623 Berlin, Germany*

[d] *Zentrum für Sonnenenergie- und Wasserstoff-Forschung Baden Württemberg (ZSW), Helmholtzstraße 8, 89081 Ulm, Germany*

## Abstract

In this study, synchrotron X-ray imaging is used to investigate the water transport inside newly developed gas diffusion media (GDM) in polymer electrolyte membrane fuel cells. Two different measurement techniques, namely in-situ radiography and quasi-in-situ tomography were combined to reveal the relationship between the structure of the microporous layer (MPL), the operation temperature and the water flow. The newly developed MPL is equipped with randomly arranged holes. It was found that these holes strongly influence the overall water transport in the whole adjacent GDM. The holes act as nuclei for water transport paths through the GDM. In the future, such tailored GDMs could be used to optimize the efficiency and operating conditions of polymer electrolyte membrane fuel cells.

*Keywords: polymer electrolyte membrane fuel cell; microporous layer; water transport; radiography; tomography; synchrotron X-ray imaging*

* Corresponding author. Tel.: +49 30 8062 42825.

E-Mail address: saad.alrwashdeh@helmholtz-berlin.de

## 1. Introduction

Fuel cells combined with electric motors are expected to offer alternatives to conventional engines powered by fossil fuels in both mobile and stationary applications [1, 2]. For transportation, and here especially in the automotive sector, polymer electrolyte membrane fuel cells (PEMFC) are considered the most promising fuel cell type.

In such PEMFC, a careful water management is crucial to prevent two unfavorable operation situations: Excessive drying of the membrane and flooding of the diffusion media [1, 3-5]. In the first case, the membrane shrinks and loses its proton conductivity, which decreases fuel cell efficiency. In the second case, liquid water in the cell materials blocks gas flow to the catalyst layers. As a consequence, the catalyst layers are undersupplied with gas and the cell performance drops. Hence, a well-balanced water management is an essential condition for optimum power output and long term stability.

Optimization of the water transport in the gas diffusion and the microporous layers leads to a better efficiency especially under critical operation conditions that promote flooding. Such conditions include temperatures below 60 °C as well as high currents that both give rise to elevated water contents [6-9]. There are many possible ways to design the gas diffusion medium (GDM), which consists of the gas diffusion layer (GDL) and, in most cases, a microporous layer (MPL). The morphology and the composition of the fiber substrate (namely the GDL) and the microporous material strongly influence water accumulation and transport [1, 10-13]. Different modeling approaches were used to analyze and optimize mass transfer within the porous materials [14-29].

Because neutrons are strongly scattered by hydrogen, imaging methods based on neutrons are very useful to investigated hydrogen distributions within a material [30-35]. For the same reason, neutron imaging is frequently used to investigate the water distribution in operating fuel cells [36-53]. Synchrotron and lab-based X-ray radiography and tomography have been used for investigation of water/media distribution with much higher spatial resolutions of a few µm, what is enough to resolve the water distribution inside the GDL pores and MPL/electrode in sufficient detail [54-69]. Recently, a more detailed understanding of the influence of GDM morphology was obtained by analyzing treated GDM materials and punching holes into the fiber substrate [70-72]. It was shown, that such GDM can significantly improve the performance of a cell [73, 74].

In this study, a modified Freudenberg MPL material with randomly arranged holes is subjected to synchrotron X-ray imaging to investigate the dynamic liquid water transport behavior. The modified material is compared to unmodified reference material at two different cell temperatures.

## 2. Experiments

The experiments were carried out using two PEMFC with active areas of 5.4 $cm^2$ and flow fields that contain seven parallel vertical channels. The first cell contains a modified membrane electrode assembly (MEA), which consists of a catalyst-coated membrane (CCM) equipped with a gas diffusion layer (GDL) from Freudenberg based on a H1411 fiber substrate, while the second cell contains a reference MEA consisting of a CCM equipped with a H1410 I4 C10 GDL. The modified GDM has an uncompressed thickness of 201 µm and includes a newly developed MPL with arbitrarily distributed holes with diameters ranging up to 30 µm. During the experiment, fuel cell operation was held at a current density of 1 A/cm² at stoichiometric ratios of 5 at both the cathode and anode sides. Cell temperatures of 40 °C and 55 °C were used and compared in this study.

The cell is investigated with synchrotron X-ray radiography and tomography of a region centered in the middle of the vertical cell extension and in an area covering ~10% of the total active area [70].

The measurements were performed at the imaging beamline “BAMline” at the synchrotron electron storage ring Bessy II in Berlin, Germany [75]. The detector contained 4008 x 2672 pixels, each 2.2 µm x 2.2 µm wide, which corresponds to the observed field of view of 8.8 mm x 5.9 mm. During radiography, images were acquired with an exposure time of 2 s. Tomographies were acquired with 3600 projection images over an angular range of 360° within a total acquisition time of about 2.5 h. A photon energy of 19 keV was selected by a W/Si double multilayer monochromator with an energy resolution $\Delta E/E$~1.5 %, ensuring sufficient transmission through the cell materials.

The beam transmission was calculated via image processing with flat field images containing the plain beam without the cell and dark field images without beam. First the cell was tomographed in the dry condition. Then, during operation, the cell was radiographed to capture the transport dynamics of the evolving liquid product water in the cell components. After the dynamic radiographic experiments, cell operation was stopped and the cell was tomographed in order to capture the water distribution inside

the fuel cell components. This technique allows for a detailed analysis of the transport dynamics, which are captured in the radiographic projection data of the three-dimensional structure of the cell materials as well as the 3D resolved water distribution during operation at a given time [76].

## 3. Results

At 40 °C, the voltage for the reference cell was 500 mV, whereas the cell with the modified material achieved 550 mV with otherwise identical operation parameters. In earlier work it was found that cracks in the MPL are seed points (nuclei) of liquid water transport paths through the GDL [76-78]. In the present case, the large MPL pores might play a similar role as the cracks: They facilitate accumulation of liquid water. The emerging product water then moves from the holes through the GDL into the channel, from where droplets are removed continuously by the gas stream. In some cases, the water is always transported through the same passage, which leads to droplets originating at the very same positions over and over again.

The tomographic image data of the dry and operated state has been matched in order to extract the water distribution. Figure 1 shows a cross section for the fuel cell (A), a cut slice in the dry state (B), the operated state (C) and the extracted water distribution (D). The slice is oriented parallel to the cell material positioned in the cathode MPL. The dry state exhibits the holes in the MPL and due to the non-uniform structure also some intruding carbon fibers. In the operated state, we find some of those holes filled with liquid water. The attenuation coefficient alone does not allow one to distinguish water and MPL material in a reliable way. However, the difference between these two states provides the water distribution as pointed out by the arrows in Figure. 1D. The tomographic data indicates that about 70% of the holes in the optimized GDM are filled with liquid water.

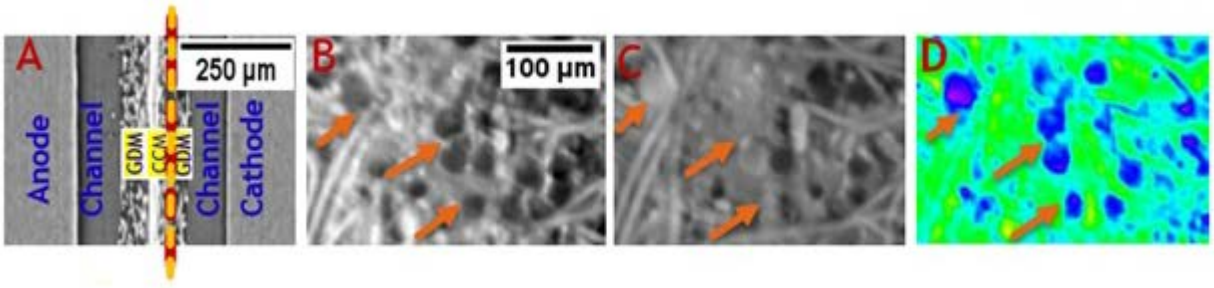


Figure. 1. (A): Cross section through the tomogram of the fuel cell. (B, C): Slices through the tomogram of the perforated MPL in the dry (B) and operated (C) state. (D): Water accumulations extracted from (B) and (C).

From the radiographic data we see that only a very few paths are used for water transport. In Figure. 2(A) we can see a water activity map and in Figure. 2(B) the water distribution of a cutout (3 mm x 1 mm) of the complete field of view, which includes three marked droplets as very active points that are building up again and again. The activity map highlights areas with strong temporal fluctuations of beam attenuation, which especially applies to the droplets. The temporal activity $A_t(x, y)$ at a given pixel position $(x, y)$ is defined as

$$A_t = \frac{1}{t*N} \sum_{k=2}^{N} | d_k(x, y) - d_{k-1}(x, y)|,$$

where N is the total number of images, $d$ the local water depth and $t$ the exposure time of each image. For pixels that do not change their grey value, $A_t = 0$ (black in Fig. 2). Pixels that fluctuate in intensity (water depth) have non-zero values (colors in Figure. 2).

Figure. 2(D) displays the water volume as a function of time for a region containing one of the droplets, see Figure. 2(C), which shows a radiographic still of droplet #3. As becomes visible in the graph, a droplet first builds up and is then carried away after some time by the gas stream. This happens periodically roughly every 30 s and results in a significant decrease of the measured water volume. The droplet grows at a rate of 0.13 nl/s, as derived from the slopes of the graph in Figure. 2(D). For droplets #1 and #2 shown in Figure. 2(B), the corresponding volume increase rate was 0.22 nl/s and 0.37 nl/s, respectively. These growth rates are related to electrochemically active areas of 0.23, 0.40 and 0.14 mm² for droplets 1, 2 and 3, respectively. Therefore, the corresponding transport paths through the GDL make an important contribution to the overall liquid water transfer through the GDL. Note that in the projection direction the complete water volume is analyzed, which includes the channels and, therefore, is subject to small variations due to water droplets passing the channel from time to time. This can be seen at the offset and short peaks in the graph (for example at 280 s).

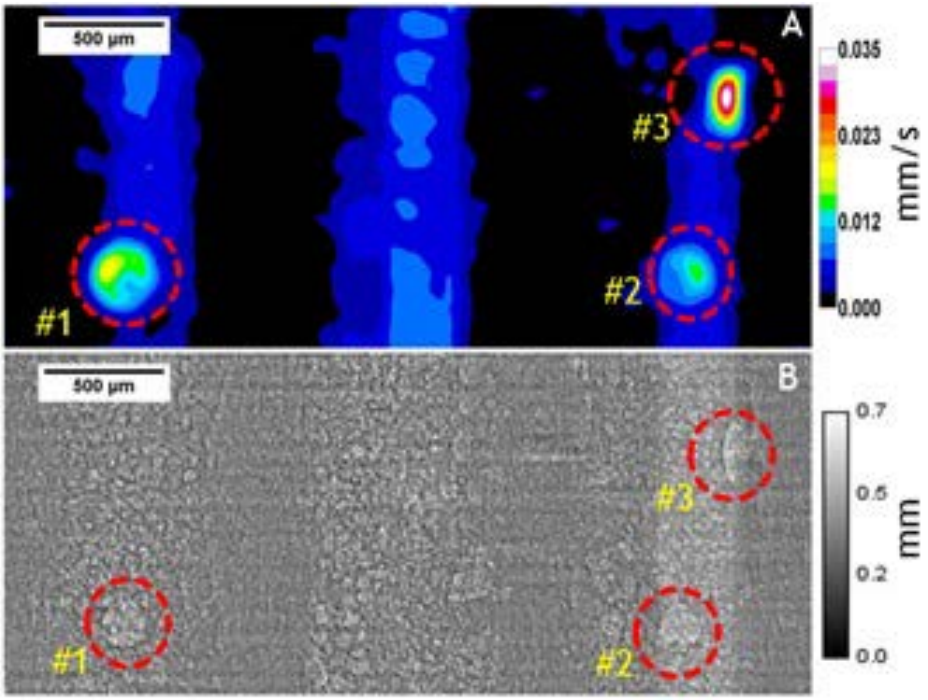


Figure. 2. Water evolution and discharge in the modified material as quantified by X-ray radiography during operation at 40 °C. (A): Activity map over 60 min of operation, (B): water distribution after 40 min of operation, (C): cut out of the area marked '#3' in (B), (D): water volume of the region containing droplet #3 as a function of time.

Figure. 3 displays water activity maps for the modified and for the reference materials at two operation temperatures, 40 °C in Figure. 3(A) and (C) and 55 °C in Figure. 3(B) and (D), respectively. The four cathodic flow field channels in the mapped area can be seen clearly because they transport large amounts of water. Bright areas (Figure. 3(A), circles) indicate the presence of well-defined fast water transport paths. In Figure. 3(B-D) no such paths were found.

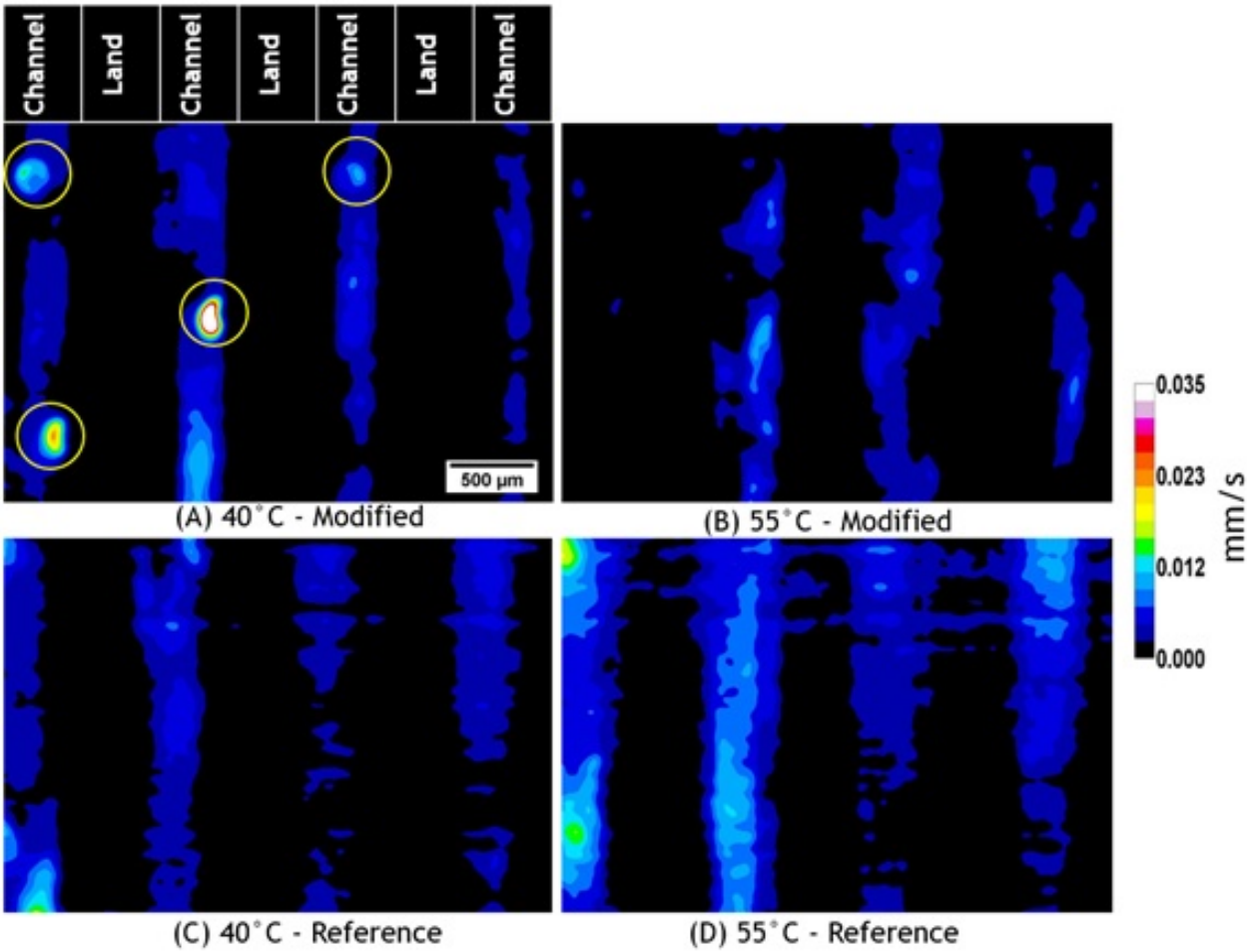


Figure. 3. Water activity maps for the modified and the reference GDM at operation temperatures of 40 °C (A and C) and 55 °C (B and D), respectively.

## 4. Discussion

The actual water production rate is the same for both operation temperatures, but for the modified GDM, the water droplets are transported differently from the GDL through the channel out of the cell. At 55 °C, see Figure. 3(B), the droplets remain at the initial position for a shorter period and take longer to move through the channel. In the corresponding activity maps of the reference material (Figure. 3(C) and Figure. 3(D)), it can be seen that liquid water moves through the cell materials at both operation temperatures without any preferred transport paths.

Therefore, it can be concluded that in comparison to the reference material operated at 40 °C the holes in the modified GDM cause the water to flow only through very few and well-defined pathways as shown in Figure. 2. The holes in the MPL act as seed points for such liquid water pathways. Compared to the reference material, these transport paths leave larger parts of the GDM free of liquid water, i.e.

more empty pore space is available for the transport of reaction gases and the supply of the catalyst. The optimized gas supply leads to an improved performance of the cell. Hence, an intentional material modification for an effective water removal from the GDL into the channel is observed.

About 70% of the holes are filled with liquid water as can be seen in the tomographic data, but only a very few transport paths are actively used. This might crucially depend on local conditions, such as adjacent pore spaces in the carbon fiber material and the non-homogeneously distributed hole positions, i.e. the water chooses always the most suited paths depending on local conditions.

The effect of the water transport path formation was only visible at 40 °C. At 55 °C, holes do not affect the liquid water transport. Due to the higher temperature the water might be mostly gaseous at the position of the MPL and therefore the effect of the holes is negligible.

The strong influence of the MPL holes on the water distribution is in general agreement with recent findings by Gerteisen et al. [73] and by Alink et al. [70, 79] who found an enhanced liquid water transport in laser-perforated GDLs. Furthermore Markötter et al.[71] and Haußmann et al. [74] have shown that water is accumulating in such laser-perforated holes within the GDL in a similar way as we have found for the MPL holes. The cyclic behavior of the water agglomerations in the holes corresponds with previous results by Litster et al., Djilali et al. and Manke et al., where an “eruptive-like” water transport mechanism through the GDL was identified [80-82].

## 5. Conclusions

This work presented a study case on a PEM fuel cell focusing on the transport of liquid water through the GDL and the channel system. Previous work has shown a strong influence of unintentionally caused cracks in the micro-porous layer and perforations of the gas diffusion media. It could be demonstrated that this effect can be at least to a certain extent exploited with a tailored GDM material containing holes in the MPL. This study shows that some of the holes in the GDM fill up with liquid water and provide nuclei of fast water transport paths through the GDL, which was not observed in the reference cell. In this way, the MPL can be used to counteract specific weak points in the flow field geometry and to optimize the overall performance of fuel cells in general.

These findings open a new perspective for material design and optimization since, for example, size, density and structure of the MPL holes can be tailored during production in analogy to other approaches to GDM design, like perforation holes through the complete GDM.

## Acknowledgements

We gratefully acknowledge the funding of the project Optigaa 2 (grant number 03ET6015A) by the Federal Ministry of Economic Affairs and Energy (BMWi.IIC6).

## References

[1] W. Vielstich, A. Lamm, H.A. Gasteiger, in, John Wiley & Sons, Chichester, 2003.
[2] G. Hoogers, in, CRC Press LLC, Boca Raton, FL,, 2003.
[3] J. Garche, C.K. Dyer, P.T. Moseley, Z. Ogumi, D.A.J. Rand, B. Scrosati, Encyclopedia of Electrochemical Power Sources, in, Elsevier, Amsterdam, 2009, pp. 4538.
[4] L. Carrette, K.A. Friedrich, U. Stimming, Fuel Cells, 1 (2001) 5-39.
[5] C.-Y. Wang, Two-phase flow and transport, in: W. Vielstich, A. Lamm, H.A. Gasteiger (Eds.) Handbook of Fuel Cells – Fundamentals, Technology and Applications, John Wiley & Sons, Chichester, 2003, pp. 337–347.
[6] Z.G. Qi, A. Kaufman, Journal of Power Sources, 109 (2002) 38-46.
[7] J.T. Gostick, M.A. Ioannidis, M.W. Fowler, M.D. Pritzker, Electrochemistry Communications, 11 (2009) 576-579.
[8] C. Quick, D. Ritzinger, W. Lehnert, C. Hartnig, Journal of Power Sources, 190 (2009) 110-120.
[9] T. Kitahara, T. Konomi, H. Nakajima, Journal of Power Sources, 195 (2010) 2202-2211.
[10] C.-Y. Wang, Chemical Reviews, 104 (2004) 4727-4766.
[11] P.K. Sinha, P.P. Mukherjee, C.Y. Wang, Journal of Materials Chemistry, 17 (2007) 3089-3103.
[12] C. Tötzke, G. Gaiselmann, M. Osenberg, J. Bohner, T. Arlt, H. Markötter, A. Hilger, F. Wieder, A. Kupsch, B.R. Müller, M.P. Hentschel, J. Banhart, V. Schmidt, W. Lehnert, I. Manke, Journal of Power Sources, 253 (2014) 123-131.
[13] J.G. Carton, V. Lawlor, A.G. Olabi, C. Hochenauer, G. Zauner, Energy, 39 (2012) 63-73.
[14] S. Cordiner, S.P. Lanzani, V. Mulone, International Journal of Hydrogen Energy, 36 (2011) 10366-10375.
[15] S. Cordiner, S.P. Lanzani, V. Mulone, M. Chiapparini, A. D'Anzi, D. Orsi, Journal of Fuel Cell Science and Technology, 6 (2009).
[16] S. Cordiner, V. Mulone, F. Romanelli, Journal of Fuel Cell Science and Technology, 4 (2007) 317-327.
[17] M. Abdollahzadeh, J.C. Pascoa, A.A. Ranjbar, Q. Esmaili, Energy, 68 (2014) 478-494.
[18] F. Al-Hadeethi, M.d. Al-Nimr, M. Al-Safadi, Energy, 90 (2015) 475-482.
[19] N. Djilali, Energy, 32 (2007) 269-280.
[20] S. Kang, Energy, 90 (2015) 1388-1400.
[21] C. Siegel, Energy, 33 (2008) 1331-1352.
[22] L. Xing, X. Liu, T. Alaje, R. Kumar, M. Mamlouk, K. Scott, Energy, 73 (2014) 618-634.
[23] G. Gaiselmann, C. Tötzke, I. Manke, W. Lehnert, V. Schmidt, Journal of Power Sources, 257 (2014) 52-64.
[24] J.G. Carton, A.G. Olabi, International Journal of Hydrogen Energy, 40 (2015) 5726-5738.
[25] J.G. Carton, A.G. Olabi, Energy, 35 (2010) 2796-2806.
[26] D. Cha, J.H. Ahn, H.S. Kim, Y. Kim, Energy, 93 (2015) 1338-1344.
[27] G. Gaiselmann, R. Thiedmann, I. Manke, W. Lehnert, V. Schmidt, Computational Materials Science, 59 (2012) 75-86.

[28] G. Gaiselmann, D. Froning, C. Tötzke, C. Quick, I. Manke, W. Lehnert, V. Schmidt, International Journal of Hydrogen Energy, 38 (2013) 8448-8460.
[29] R. Thiedmann, V. Schmidt, I. Manke, W. Lehnert, Royal Statistical Society - Series C: Applied Statistics, in press (2011).
[30] J. Banhart, in, Oxford University Press, Oxford, UK, 2008.
[31] K. Herbrig, C. Pohlmann, L. Gondek, H. Figiel, N. Kardjilov, A. Hilger, I. Manke, J. Banhart, B. Kieback, L. Roentzsch, Journal of Power Sources, 293 (2015) 109-118.
[32] C. Pohlmann, K. Herbrig, L. Gondek, N. Kardjilov, A. Hilger, H. Figiel, J. Banhart, B. Kieback, I. Manke, L. Roentzsch, Journal of Power Sources, 277 (2015) 360-369.
[33] L. Gondek, N.B. Selvaraj, J. Czub, H. Figiel, D. Chapelle, N. Kardjilov, A. Hilger, I. Manke, International Journal of Hydrogen Energy, 36 (2011) 9751-9757.
[34] A. Griesche, E. Dabah, T. Kannengiesser, N. Kardjilov, A. Hilger, I. Manke, Acta Materialia, 78 (2014) 14-22.
[35] I. Manke, J. Banhart, A. Haibel, A. Rack, S. Zabler, N. Kardjilov, A. Hilger, A. Melzer, H. Riesemeier, Applied Physics Letters, 90 (2007) 214102.
[36] R.J. Bellows, M.Y. Lin, M. Arif, A.K. Thompson, D. Jacobson, Journal of The Electrochemical Society, 146 (1999) 1099 - 1103.
[37] R. Satija, D.L. Jacobson, M. Arif, S.A. Werner, Journal of Power Sources, 129 (2004) 238-245.
[38] X. Wang, T.V. Nguyen, D.S. Hussey, D.L. Jacobson, Journal of The Electrochemical Society, 157 (2010) B1777-B1782.
[39] P. Boillat, D. Kramer, B.C. Seyfang, G. Frei, E. Lehmann, G.G. Scherer, A. Wokaun, Y. Ichikawa, Y. Tasaki, K. Shinohara, Electrochemistry Communications, 10 (2008) 546-550.
[40] E.H. Lehmann, P. Boillat, G. Scherrer, G. Frei, Nuclear Instruments and Methods in Physics Research Section A: Accelerators, Spectrometers, Detectors and Associated Equipment, 605 (2009) 123–126.
[41] A.B. Geiger, A. Tsukada, E. Lehmann, P. Vontobel, A. Wokaun, G.G. Scherer, Fuel Cells, 2 (2003) 92–98.
[42] M.C. Hatzell, A. Turhan, S. Kim, D.S. Hussey, D.L. Jacobson, M.M. Mench, Journal of The Electrochemical Society, 158 (2011) B717-B726.
[43] N. Pekula, K. Heller, P.A. Chuang, A. Turhan, M.M. Mench, J.S. Brenizer, K. Ünlü, Nuclear Instruments and Methods in Physics Research Section A: Accelerators, Spectrometers, Detectors and Associated Equipment, 542 (2005) 134-141.
[44] A.K. Heller, L. Shi, J.S. Brenizer, M.M. Mench, Nuclear Instruments and Methods in Physics Research Section A: Accelerators, Spectrometers, Detectors and Associated Equipment, 605 (2009) 99-102.
[45] H. Markotter, I. Manke, R. Kuhn, T. Arlt, N. Kardjilov, M.P. Hentschel, A. Kupsch, A. Lange, C. Hartnig, J. Scholta, J. Banhart, Journal of Power Sources, 219 (2012) 120-125.
[46] C. Totzke, I. Manke, A. Hilger, G. Choinka, N. Kardjilov, T. Arlt, H. Markotter, A. Schroder, K. Wippermann, D. Stolten, C. Hartnig, P. Kruger, R. Kuhn, J. Banhart, Journal of Power Sources, 196 (2011) 4631-4637.
[47] T. Arlt, W. Lueke, N. Kardjilov, J. Banhart, W. Lehnert, I. Manke, Journal of Power Sources, 299 (2015) 125-129.
[48] A. Iranzo, P. Boillat, P. Oberholzer, J. Guerra, Energy, 68 (2014) 971-981.
[49] A. Santamaria, H.-Y. Tang, J.W. Park, G.-G. Park, Y.-J. Sohn, International Journal of Hydrogen Energy, 37 (2012) 10836-10843.
[50] M. Weiland, P. Boillat, P. Oberholzer, A. Kaestner, E.H. Lehmann, T.J. Schmidt, G.G. Scherer, H. Reichl, Electrochimica Acta, 87 (2013) 567-574.
[51] A.D. Santamaria, M.K. Becton, N.J. Cooper, A.Z. Weber, J.W. Park, Journal of Power Sources, 293 (2015) 162-169.
[52] J.R. Bunn, D. Penumadu, R. Woracek, N. Kardjilov, A. Hilger, I. Manke, S. Williams, Applied Physics Letters, 102 (2013) 234102.
[53] M. Klages, S. Enz, H. Markotter, I. Manke, N. Kardjilov, J. Scholta, Journal of Power Sources, 239 (2013) 596-603.
[54] I. Manke, C. Hartnig, M. Grunerbel, W. Lehnert, N. Kardjilov, A. Haibel, A. Hilger, J. Banhart, H. Riesemeier, Applied Physics Letters, 90 (2007) 174105.
[55] P. Deevanhxay, T. Sasabe, S. Tsushima, S. Hirai, International Journal of Hydrogen Energy, 36 (2011) 10901-10907.
[56] J. Lee, J. Hinebaugh, A. Bazylak, Journal of Power Sources, 227 (2013) 123-130.
[57] J. Hinebaugh, J. Lee, A. Bazylak, Journal of The Electrochemical Society, 159 (2012) F826-F830.

[58] C. Hartnig, I. Manke, J. Schloesser, P. Krüger, R. Kuhn, H. Riesemeier, K. Wippermann, J. Banhart, Electrochemistry Communications, 11 (2009) 1559-1562.
[59] J. Lee, R. Yip, P. Antonacci, N. Ge, T. Kotaka, Y. Tabuchi, A. Bazylak, Journal of the Electrochemical Society, 162 (2015) F669-F676.
[60] J. Eller, J. Roth, F. Marone, M. Stampanoni, A. Wokaun, F.N. Buechi, Journal of Power Sources, 245 (2014) 796-800.
[61] R. Kuhn, J. Scholta, P. Krueger, C. Hartnig, W. Lehnert, T. Arlt, I. Manke, Journal of Power Sources, 196 (2011) 5231-5239.
[62] T. Sasabe, S. Tsushima, S. Hirai, International Journal of Hydrogen Energy, 35 (2010) 11119-11128.
[63] A. Bazylak, International Journal of Hydrogen Energy, 34 (2009) 3845-3857.
[64] A. Lange, A. Kupsch, M.P. Hentschel, I. Manke, N. Kardjilov, T. Arlt, R. Grothausmann, Journal of Power Sources, 196 (2010) 5293-5298.
[65] W. Maier, T. Arlt, K. Wippermann, C. Wannek, I. Manke, W. Lehnert, D. Stolten, Journal of The Electrochemical Society, 159 (2012) F398-F404.
[66] S.H. Eberhardt, F. Marone, M. Stampanoni, F.N. Buchi, T.J. Schmidt, J. Synchrot. Radiat., 21 (2014) 1319-1326.
[67] P.K. Sinha, P. Halleck, C.-Y. Wang, Electrochemical and Solid-State Letters, 9 (2006) A344-A348.
[68] T. Arlt, A. Schroeder, K. Heyne, H. Riesemeier, K. Wippermann, W. Lehnert, I. Manke, Journal of Power Sources, 297 (2015) 83-89.
[69] T. Arlt, I. Manke, K. Wippermann, H. Riesemeier, J. Mergel, J. Banhart, Journal of Power Sources, 221 (2013) 210-216.
[70] R. Alink, J. Haußmann, H. Markötter, M. Schwager, I. Manke, D. Gerteisen, Journal of Power Sources, 233 (2013) 358-368.
[71] H. Markotter, R. Alink, J. Haussmann, K. Dittmann, T. Arlt, F. Wieder, C. Totzke, M. Klages, C. Reiter, H. Riesemeier, J. Scholta, D. Gerteisen, J. Banhart, I. Manke, International Journal of Hydrogen Energy, 37 (2012) 7757-7761.
[72] J. Haussmann, H. Markotter, R. Alink, A. Bauder, K. Dittmann, I. Manke, J. Scholta, Journal of Power Sources, 239 (2013) 611-622.
[73] D. Gerteisen, T. Heilmann, C. Ziegler, Journal of Power Sources, 177 (2008) 348-354.
[74] J. Haußmann, H. Markötter, R. Alink, A. Bauder, K. Dittmann, I. Manke, J. Scholta, Journal of Power Sources, 239 (2013) 611-622.
[75] W. Görner, M.P. Hentschel, B.R. Müller, H. Riesemeier, M. Krumrey, G. Ulm, W. Diete, U. Klein, R. Frahm, Nuclear Instruments and Methods in Physics Research Section A: Accelerators, Spectrometers, Detectors and Associated Equipment, 467-468 (2001) 703-706.
[76] P. Krüger, H. Markötter, J. Haußmann, M. Klages, T. Arlt, J. Banhart, C. Hartnig, I. Manke, J. Scholta, Journal of Power Sources, 196 (2011) 5250-5255.
[77] H. Markotter, J. Haussmann, R. Alink, C. Totzke, T. Arlt, M. Klages, H. Riesemeier, J. Scholta, D. Gerteisen, J. Banhart, I. Manke, Electrochemistry Communications, 34 (2013) 22-24.
[78] T. Sasabe, P. Deevanhxay, S. Tsushima, S. Hirai, Electrochemistry Communications, 13 (2011) 638-641.
[79] R. Alink, D. Gerteisen, W. Mérida, Fuel Cells, 11 (2011) 481-488.
[80] S. Litster, D. Sinton, N. Djilali, Journal of Power Sources, 154 (2006) 95-105.
[81] I. Manke, C. Hartnig, N. Kardjilov, H. Riesemeier, J. Goebbels, R. Kuhn, P. Krüger, J. Banhart, Fuel Cells, 10 (2010) 26-34.
[82] N. Djilali, P.C. Sui, International Journal of Computational Fluid Dynamics, 22 (2008) 115-133.